

Understanding Human Fall from Standing via Whole-body Musculoskeletal Simulation

Chengtian Ma, Yunyue Wei, Chenhui Zuo, Chen Zhang, Yanan Sui

Abstract—Understanding human standing and falling is crucial for advancing the design of assistive robots and human-like bipedal robots. Due to the ethical and practical challenges of conducting human fall experiments, this study employs a high-dimensional musculoskeletal model with a comprehensive set of skeletal muscles, to simulate the transition from standing to falling. We investigate the intrinsic temporal dynamics, motor responses, and distribution of related metrics across the human body during balance loss. By exploring the complex dynamical space of standing and falling via large-scale simulation, we identify biologically plausible fall patterns and key factors that influence fall behaviors. These findings contribute to a deeper, quantitative understanding of human falling from standing.

I. INTRODUCTION

Humans rely on an obligate bipedal stance, requiring precise coordination between the musculoskeletal and neural systems [1]. Unlike bipedal robots, human balance control exhibits remarkable adaptability and resilience, but its underlying principles remain an open question in biomechanics and robotics. A full-body musculoskeletal model provides the necessary foundation to investigate fine-grained, muscle-level postural dynamics essential to human standing [2].

As the counterpart to balancing, falling is a leading cause of injury-related deaths, particularly among older adults and individuals with movement disorders. Understanding falling dynamics is critical for identifying biomechanical risk factors and developing prevention strategies [3], [4]. Existing datasets [5], [6] primarily consist of voluntary falls, which differ substantially from real-world falls in terms of impact dynamics and protective responses [7]. Although there are studies of fall simulation aimed to tackle data scarcity, they are limited to simplified models [8], [9] or interaction modeling without whole-body dynamical movement [10].

To address these challenges, we introduce a hierarchical control and analysis pipeline for the MS-Human-700 musculoskeletal model [11], enabling controlled simulations of balance and falls with biomechanical fidelity. Our contributions include:

- A hierarchical control and analysis pipeline over a comprehensive human musculoskeletal model to enable controlled balance and fall simulation with biomechanical fidelity.
- Large-scale generation of balancing behaviors, revealing whole-body stability dynamics.
- Statistical analysis of fall factors, offering insights into human motor control and fall prevention.

The authors are with the School of Aerospace Engineering, Tsinghua University, Beijing, China. Correspondence to Yanan Sui. E-mail: ysui@tsinghua.edu.cn

II. BIPEDAL POSTURAL CONTROL

A. Musculoskeletal Model Dynamics

The musculoskeletal model used in this work is the MS-Human-700 model [11]. It comprises of 90 rigid body segments, 206 joints and 700 muscle-tendon units. By actuating its 700 muscle-tendon units, the model can be controlled and perform human-like tasks.

MS-Human-700 model is implemented in the MuJoCo physics engine [12]. The actuators of the model in this work are 700 Hill-type [13] muscles. The actuator force generated by each muscle-tendon unit, and the temporal relation between muscle activation act and the input control signal of the musculoskeletal model u can be decided by the following equations:

$$f_m(act) = f_{max} \cdot [F_l(l_m) \cdot F_v(v_m) \cdot act + F_p(l_m)]. \quad (1)$$

$$\frac{\partial act}{\partial t} = \frac{u - act}{\tau(u, act)}. \quad (2)$$

F_l and F_v are force-length and force-velocity functions, F_p is the passive force, and l_m, v_m are normalized muscle length and velocity. f_{max} is the maximum isometric muscle force. Muscle activation act is calculated with control u in the first-order nonlinear system in Eq. (2) [14].

B. Postural PD Control over Muscles

To tackle the very high dimensionality of musculoskeletal model postural control, a normalized PD control-like formulation over muscle lengths is used to derive desired muscle forces [15], written as:

$$f_m = \min(0, k_p \cdot (l_m^* - l_m) / l_{range} + k_d \cdot (0 - \dot{l}_m)), \quad (3)$$

where f_m stands for muscle forces, k_p and k_d are PD control gains, l_m stands for actual muscle lengths, \dot{l}_m stands for muscle velocities and l_m^* is target muscle lengths. The difference between the maximum muscle length and the minimum muscle length of each muscle, l_{range} , is used to normalize muscle lengths and stabilize control effect.

To fully control the musculoskeletal model after obtaining desired muscle forces, inverse dynamics of the muscles are applied to get the control that generates desired muscle activation in the time step.

III. STANDING AND FALLING SIMULATION

A. Standing Task Design

We treat the human standing control problem as a finite horizon Markov decision process with state $s \in \mathcal{S}$, control $u \in \mathcal{U}$, dynamics $s_{t+1} = f(s_t, u_t)$, and time step t . For

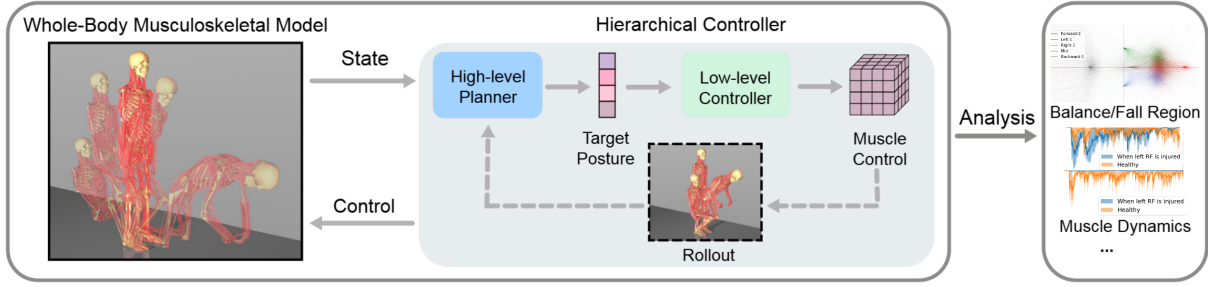


Fig. 1: Control and analysis of the human musculoskeletal model standing and falling.

a given initial state s_0 and a desired standing horizon T , we aim to find a control sequence $U_T^* = (u_0, \dots, u_{T-1})$ that successfully maintains the standing posture by minimizing a pre-defined cost function C :

$$U_T^* = \operatorname{argmin}_{U_T} \sum_{t=0}^{T-1} C(s_t, u_t) \quad (4)$$

The control goal for standing is: (1) Near-zero CoM horizontal velocity and (2) Zero moment point (ZMP) within the support region, ensuring no flipping tendency. The model may step for balance, but its initial position remains constant across experiments.

B. Hierarchical Balance Control

We propose Hierarchical Balance Control (HBC), a hierarchical balance control method for human body. As shown in Figure 1, a high-level planner first proposes a set of 37 major joint coordinates $z^* \in \mathcal{Z}$ as the low-level control target. Given target joint angles and the model dynamics f , the muscle-level PD controller introduced in section II works as the low-level controller to coordinate muscles to adjust the target posture. HBC reduces the parameter space from the scale of muscle number to joint number. Compared to MuscleVAE [15] which also applied PD control over muscles, our approach focuses on balance and leverages available model dynamics for efficient sampling.

HBC utilizes model predictive control (MPC) to optimize the target joint coordinates according to the cost function over a fixed horizon:

$$z^* = \operatorname{argmin}_z \sum_{t=t_p}^{t_p+H-1} C(s_t, u_t), u_t = \mathcal{PD}(s_t, z), \quad (5)$$

where $t_p = \{t \mid t \bmod t_e = 0\}$ is the planning timestep and $H \ll T$ is the planning horizon.

We integrate Model Predictive Path Integral (MPPI, [16]) as the high-level planner into HBC as follows:

1) *Rollout process*: At the beginning of each rollout process, N sets of target joint angles z_1, z_2, \dots, z_N are sampled from the current target distribution $\mathcal{N}(\mu, \sigma)$ to generate N trajectories. The cumulative cost $c_n = \sum_{t=t_p}^{t_p+H-1} C(s_t, \mathcal{PD}(s_t, z_n))$ is calculated from the rollout trajectory of target z_n .

Algorithm 1: Hierarchical Balance Control (HBC)

Input: Model dynamics f , total time steps T , execution length t_e , rollout horizon h , particle number n , MPPI iteration number r , initial distribution parameter μ, σ

Output: Action sequence U^*

```

1  $s_0 \sim \mathcal{S}_0, U^* \leftarrow \emptyset$ 
2 for  $t = 0, \dots, T-1$  do
3   if  $t \bmod t_e = 0$  then
4     for  $i = 1, \dots, r$  do
5        $z_1, \dots, z_N \sim \mathcal{N}(\mu, \sigma)$ 
6        $c_1, \dots, c_n \leftarrow \text{Rollout}(z_1, \dots, z_n)$ 
7       Update  $\mu, \sigma$  using e.q. (6)
8     end
9      $z^* \sim \mathcal{N}(\mu, \sigma)$ 
10  end
11   $u_t \leftarrow \mathcal{PD}(s_t, z^*)$ 
12   $U^* = U^* \cup u_t$ 
13   $s_{t+1} \leftarrow f(s_t, u_t)$ 
14 end

```

2) *Distribution update*: The new mean and covariance are calculated based on the weighted average of top k targets ($z_1^*, z_2^*, \dots, z_k^*$) whose corresponding trajectories return the minimal costs. The update is implemented as follows:

$$\mu = \frac{\sum_{j=1}^k w_j \cdot z_j^*}{\sum_{j=1}^k w_j}, \sigma = \sqrt{\frac{\sum_{j=1}^k w_j \cdot (z_j^* - \mu)^2}{\sum_{j=1}^k w_j}}, \quad (6)$$

where $w_j = e^{-\frac{1}{\lambda} c_j}$ is the aggregate weight for z_j , and λ is the softmax temperature. The full pipeline of getting control sequences is as Algorithm 1.

C. Fall from Standing Simulation

We extend simulated scenarios to standing which is likely followed by a fall, by modeling the balance loss in populations who are prone to falling. We model three categories of falling-prone factors:

(1) **Fall with muscle injury**. To simulate muscle strain, we restrict the range of force applied to the left Rectus Femoris (RF). (2) **Fall with neuronal control latency**. By modeling a 50% reduction in high-level planning frequency, we simulate this age-related neuronal latency [17], providing insights into

its role in balance impairments and fall risk. **(3) Fall with muscle weakness.** We model the muscle strength loss due to aging [18] by down-regulating the maximum force of each muscle to 50% of the original value.

IV. EXPERIMENTS

A. Control Performance Evaluation

HBC successfully solves the standing control task on a high-dimensional, over-actuated system. We compare HBC with Dynamic Synergy Representation (DynSyn), the leading DRL-based control method for musculoskeletal systems [19], trained with the same cost function over 30 million steps and three random seeds. Compared to Deep Reinforcement Learning (DRL) based methods, HBC is training free and can generalize to various conditions. Additionally, MPPI [16] is included in an ablation study of our hierarchical control pipeline. Figure 2a shows that our approach significantly outperforms both alternatives, achieving longer stable standing durations.

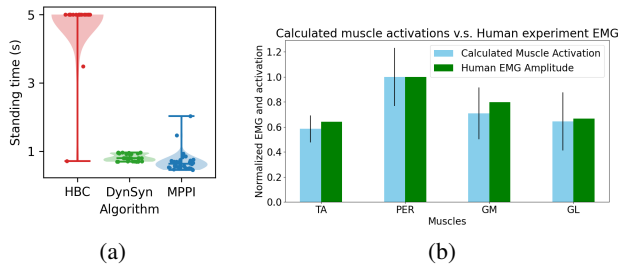


Fig. 2: Baseline comparison and fidelity check. (a) Standing duration performance over 30 independent trials for each methods. (b) The activation of calf muscles (calculated with control of muscles) in standing simulation show good consistency with EMG ground truth in biomechanical experiments. Notes: TA, tibialis anterior; PER, peroneus; GM, gastrocnemius medialis; GL, gastrocnemius lateralis. The RMS of EMG and activation are normalized by their max value in four muscles.

We carry out a fidelity check on our simulation results by comparing the activation calculated by HBC control over muscles during standing with the root mean square (RMS) values of electromyography (EMG) signals from calf muscles during standing tasks as reported in [20] [21]. Figure 2b shows that the simulation results demonstrate consistency with real-world experiments.

B. Experiment Settings

1) *Balancing behavior analysis:* We apply HBC over the healthy MS-Human-700 model starting from a natural standing initial posture for 5 seconds and monitor CoM-related metric to observe the model’s dynamical behavior.

2) *Falling detection and recording:* We apply HBC on the modified model from an up-straight posture for 5 seconds with falling-prone factors. The human model has a much higher possibility to fall from standing.

We track the CoM position of the model and the support polygon formed by heels and toes. The initialization event occurs when the CoM crosses from inside to outside the support polygon, marking the start of falling. The contact event is defined as the moment when the body-ground contact force reaches its peak, indicating impact.

During the 5-second trial, these events determine the model’s balance status: the initialization event signals the start of a fall, while the contact event marks ground collision. We define fall duration as the time between these two events.

C. Study of Standing Dynamics

For all plots on a coordinate plane, the X-axis points to the front of the human body, the Y-axis points to the left side, and the positive Z-axis points to the upward vertical direction.

1) *CoM movements from various initial postures:* We initialize the MS-Human-700 model in six different postures while maintaining the same foot positions to observe CoM trajectories.

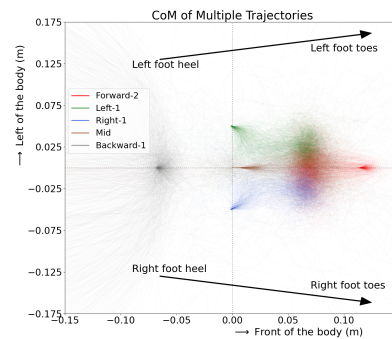


Fig. 3: (a) Trajectories of CoM horizontal position during standing task starting from different postures (Forward-2, Left-1, Right-1, Mid and Backward-1).

Figure 3 highlights a balance region during standing. Most CoM trajectories converge in front of the feet. In contrast, the divergence from Backward-1 and strong recovery from Forward-2 suggest greater sensitivity to backward leaning.

D. The Falling Dynamics

This section presents the falling behavior collected from models with three falling-prone factors introduced in Section III-C. The origin of coordinates refer to the position of pelvis, and the initial position of the CoM is indicated on each plot for better clarity.

1) *Model behavior under falling-prone factors:* Figure 4a shows that models with muscle force loss have shorter average fall durations and reduced duration variance. Figure 4b shows a significant increase in right RF muscle force during balance maintenance, suggesting a weight shift to the right leg for stability.

2) *The distribution of falling behavior:* Falling behavior in musculoskeletal models varies in direction, contact points, and duration, following a statistically meaningful pattern under a fixed control policy.

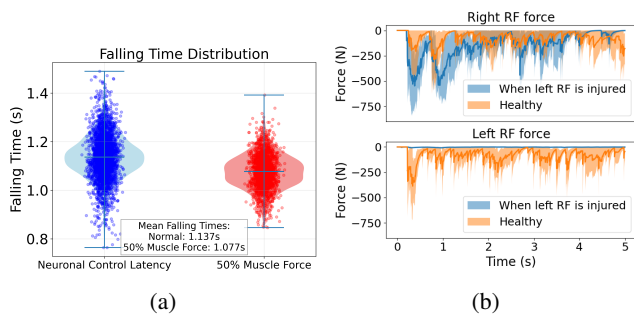


Fig. 4: (a) The distribution of fall duration for falling due to neuronal latency and muscle force loss. (b) Right side RF force when performing standing task with injury present on the left side RF.

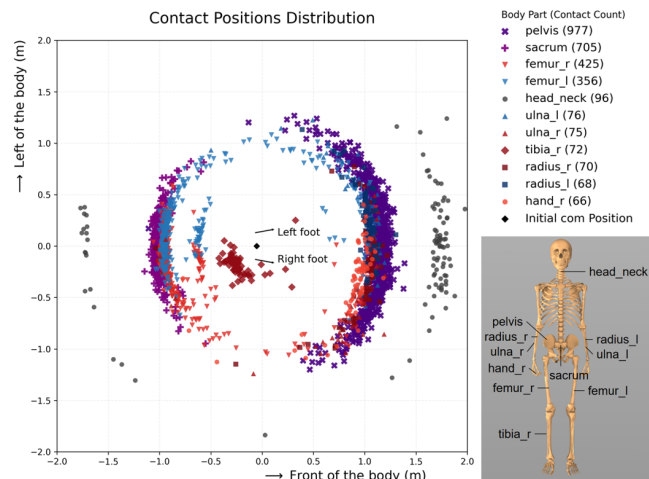


Fig. 5: Distribution of Contact Positions after Falling. “l” and “r” refer to the left and right side of the body.

Post-fall contact locations correlate with injury risk, offering insights that are challenging to obtain from real-world experiments. Figure 5 shows the contact distribution in models with neuronal control latency, with frequent impacts at the pelvis, thighs, and head. This aligns with clinical data, where hip fractures—accounting for 68% of fall-related injuries—are a major concern [22]. Over 95% of hip fractures in the elderly result from falls, with the pelvis and proximal femur being most vulnerable [23]. Head injuries also pose significant long-term risks. Understanding these contact patterns helps identify biomechanical injury factors, aiding fall prevention and protective strategies.

E. Falling Behavior Variance with Motor Dysfunctions

Figure 6 shows fall duration changes with muscle force loss. In the full-force model with neuronal latency, longer falls occur more often backward. With 50% muscle force loss, longer falls shift forward, and fall duration variability decreases.

Figure 7 gives supplementary details on the frequency of falling happening on different directions. We segment falling direction by tracking the contact position, and divide the X-Y plane into 4 areas, each possessing a 90 degrees span. For

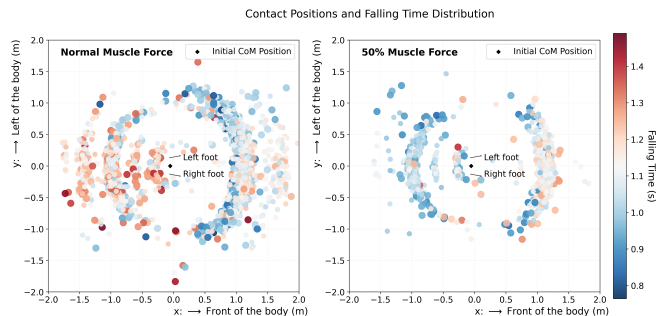


Fig. 6: The scatter plot of contact positions after falling due to neuronal latency and muscle force loss. Scatter positions refer to the first contact happening between body and the ground, and colors of scatter points indicate the fall duration.

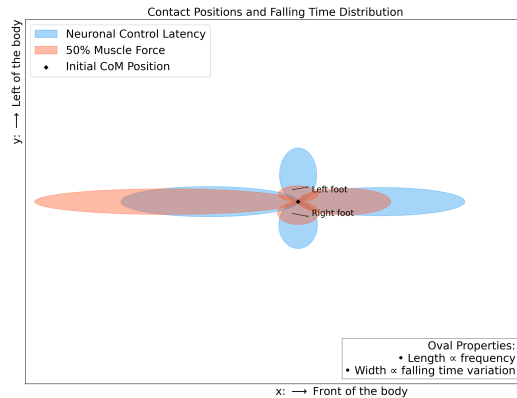


Fig. 7: The fall duration and direction of MS-Human-700 model with control latency and 50% muscle force loss. The length of each oval is proportional to the percentage frequency of falling on each direction, while the width of each oval is proportional to the variance of fall duration.

the 50% muscle force model, it is easier for the model to fall backward with a smaller variance of fall duration, while the frequency of lateral falling is reduced.

V. CONCLUSION

We introduce a high-dimensional control pipeline for stable standing in a full-body musculoskeletal model. By analyzing CoM trajectories and balance regions across various conditions, we uncover whole-body stability dynamics. Our study provides statistical insights into fall duration, contact distribution, and the effects of muscle injury, neuronal latency, and force loss. These findings enhance our understanding of balance mechanisms, aiding bio-inspired robotics, personalized fall-prevention and rehabilitation strategies. The ground contact simulation uses simplified mesh contact, which is computationally efficient. Future work will include better modeling of the mechanical interface between the ground and human tissue to reflect the impact of collision due to falls.

REFERENCES

- [1] J. R. Skoyles, "Human balance, the evolution of bipedalism and dysequilibrium syndrome," *Medical Hypotheses*, vol. 66, no. 6, pp. 1060–1068, 2006.
- [2] F. J. Valero-Cuevas, H. Hoffmann, M. U. Kurse, J. J. Kutch, and E. A. Theodorou, "Computational models for neuromuscular function," *IEEE reviews in biomedical engineering*, vol. 2, pp. 110–135, 2009.
- [3] R. Gelbard, K. Inaba, O. T. Okoye, M. Morrell, Z. Saadi, L. Lam, P. Talving, and D. Demetriades, "Falls in the elderly: a modern look at an old problem," *The American Journal of Surgery*, vol. 208, no. 2, pp. 249–253, 2014.
- [4] P. Nisipeanu and R. Inzelberg, "Falls in elderly people," *The Lancet*, vol. 349, no. 9059, p. 1180, 1997.
- [5] E. Hsiao and S. Robinovitch, "Common protective movements govern unexpected falls from standing height," *Journal of Biomechanics*, vol. 31, no. 1, 1997.
- [6] W. et al., "Kinematic analysis of video-captured falls experienced by older adults in long-term care," *Journal of Biomechanics*, vol. 48, no. 6, 2015.
- [7] e. a. J. Klenk, "Comparison of acceleration signals of simulated and real-world backward falls," *Medical Engineering Physics*, vol. 33, no. 3, 2011.
- [8] G. Pascoletti, D. Catelani, P. Conti, F. Cianetti, and E. M. Zanetti, "A multibody simulation of a human fall: model creation and validation," *Procedia Structural Integrity*, vol. 24, pp. 337–348, 2019.
- [9] G. Mastorakis, T. Ellis, and D. Makris, "Fall detection without people: A simulation approach tackling video data scarcity," *Expert Systems with Applications*, vol. 112, pp. 125–137, 2018.
- [10] S. Han, X. Jiang, and Y. Gao, "Human fall simulation testing method: where we are," *Osteoporosis International*, vol. 36, no. 1, pp. 35–45, 2025.
- [11] C. Zuo, K. He, J. Shao, and Y. Sui, "Self model for embodied intelligence: Modeling full-body human musculoskeletal system and locomotion control with hierarchical low-dimensional representation," in *2024 IEEE International Conference on Robotics and Automation (ICRA)*, 2024, pp. 13 062–13 069.
- [12] E. Todorov, T. Erez, and Y. Tassa, "Mujoco: A physics engine for model-based control," in *2012 IEEE/RSJ International Conference on Intelligent Robots and Systems*, 2012, pp. 5026–5033.
- [13] F. E. Zajac, "Muscle and tendon: properties, models, scaling, and application to biomechanics and motor control," *Critical reviews in biomedical engineering*, vol. 17, no. 4, pp. 359–411, 1989.
- [14] M. Millard, T. Uchida, A. Seth, and S. L. Delp, "Flexing computational muscle: modeling and simulation of musculotendon dynamics," *Journal of biomechanical engineering*, vol. 135, no. 2, p. 021005, 2013.
- [15] Y. Feng, X. Xu, and L. Liu, "Musclevae: Model-based controllers of muscle-actuated characters," 2023. [Online]. Available: <https://arxiv.org/abs/2312.07340>
- [16] G. Williams, P. Drews, B. Goldfain, J. M. Rehg, and E. A. Theodorou, "Aggressive driving with model predictive path integral control," in *2016 IEEE International Conference on Robotics and Automation (ICRA)*, 2016, pp. 1433–1440.
- [17] D. A. Bolton and J. K. Richardson, "Inhibitory control and fall prevention: why stopping matters," *Frontiers in neurology*, vol. 13, p. 853787, 2022.
- [18] U. Granacher, L. Zahner, and A. Gollhofer, "Strength, power, and postural control in seniors: Considerations for functional adaptations and for fall prevention," *European Journal of Sport Science*, vol. 8, no. 6, pp. 325–340, 2008.
- [19] K. He, C. Zuo, C. Ma, and Y. Sui, "Dynsyn: Dynamical synergistic representation for efficient learning and control in overactuated embodied systems," 2024. [Online]. Available: <https://arxiv.org/abs/2407.11472>
- [20] M. Blaszczyzyn, A. Szczesna, and K. Piechota, "semg activation of the flexor muscles in the foot during balance tasks by young and older women: A pilot study," *International journal of environmental research and public health*, vol. 16, no. 22, p. 4307, 2019.
- [21] E. Yamanaka, Y. Horiuchi, and I. Nojima, "Emg-emg coherence during voluntary control of human standing tasks: a systematic scoping review," *Frontiers in Neuroscience*, vol. 17, p. 1145751, 2023.
- [22] P. Kannus, J. Parkkari, S. Koskinen, S. Niemi, M. Palvanen, M. Järvinen, and I. Vuori, "Fall-induced injuries and deaths among older adults," *Jama*, vol. 281, no. 20, pp. 1895–1899, 1999.
- [23] R. Vaishya and A. Vaish, "Falls in older adults are serious," *Indian journal of orthopaedics*, vol. 54, pp. 69–74, 2020.